

# Symmetry energies, pairing energies, and mass equations

J. Jänecke<sup>a,\*</sup>, T.W. O'Donnell<sup>b</sup>

<sup>a</sup> *Department of Physics, University of Michigan, Ann Arbor, MI 48109-1040, USA*

<sup>b</sup> *Michigan Center for Theoretical Physics and Residential College, Science, Technology and Society Program, University of Michigan, Ann Arbor, MI 48109-1245, USA*

Received 1 April 2006; received in revised form 1 November 2006; accepted 2 November 2006

Available online 29 November 2006

---

## Abstract

Symmetry and pairing energies of atomic nuclei are related to the differences between the excitation energies of isobaric analog states in the same nucleus. Numerous such excitation energies are known experimentally. In addition, a comprehensive global set can be deduced from the available experimental masses by applying Coulomb energy corrections. Replacing the experimental mass data by available theoretical mass predictions as basis for this procedure to extract symmetry and pairing energies makes it possible to directly compare theoretical and experimental quantities. These comparisons reflect upon the goodness or possible shortcomings of the respective mass equation since symmetry energies are related to the curvature of the nuclear mass surface. A discussion of eleven selected mass equations or procedures for reproducing experimental masses and extrapolating into regions of unknown nuclei is presented.

© 2006 Elsevier B.V. All rights reserved.

PACS: 21.10.Dr; 21.10.Hw; 21.30.Fe; 21.60.-n

Keywords: NUCLEAR STRUCTURE  $Z = 1-118$ ; analyzed isobaric analog states energies, related data; deduced pairing and symmetry energy systematics. Comparisons with theoretical mass predictions and extrapolations.

---

## 1. Introduction

Numerous theoretical approaches have been employed to develop equations and procedures to calculate masses and binding energies of atomic nuclei. The reliability of extrapolations into

---

\* Corresponding author.

E-mail address: [janecke@umich.edu](mailto:janecke@umich.edu) (J. Jänecke).

regions of unknown nuclei is of interest for many aspects of nuclear structure and is particularly important for astrophysical applications. Neutron-rich and proton-rich nuclei participate in various astrophysical processes. These include explosive burning processes in light nuclei including rapid proton capture, and the slow and rapid neutron capture processes which are responsible for the production of heavy nuclei.

An overview of the trends to determine nuclear masses, both experimentally and theoretically, has been reported recently [1]. The authors classify the theoretical equations as follows: (A) the semi-empirical liquid-drop-model mass formula, (B) microscopic approaches, (C) macroscopic-microscopic approaches, (D) other global approaches, and (E) local mass formulae.

The quality of the various approaches in reproducing the experimental masses and extrapolating into regions of unknown nuclei is generally judged by two criteria. The physical concepts and theoretical techniques which enter into the various approaches must be considered and evaluated. In addition, experimental and calculated mass values have to be compared. This is usually done by comparing newly measured mass values with the predicted values. Such a procedure is by necessity often limited to nuclei close to the known nuclei. Three mass equations [2–5] are currently considered to provide the most reliable extrapolations.

Another approach is taken in the present work to compare experimental masses and theoretical mass predictions. Here, symmetry energies are considered. These represent higher-order quantities related to the curvature of the nuclear mass surface with respect to increasing neutron excess. Very preliminary results have been reported previously [6].

Relationships have been established between symmetry energies  $E_{\text{sym}}(A, T)$  and pairing energies  $P(A, T)$  of atomic nuclei on the one hand, and the energy differences  $\Delta_{T',T}(A)$  on the other [7,8]. Here, the energies  $\Delta_{T',T}(A)$  are the differences in excitation energy between the energetically lowest states with isospins  $T'$  and  $T$  in the same nucleus. These are states which are either ground states or states analog to ground states in neighboring isobars. These connections make it possible to establish interesting isospin-related properties of nuclear binding energies and masses [8].

Given that symmetry and pairing energies can be obtained globally from experimental binding energies, the same procedures can also be used to extract these quantities for theoretical mass equations. Comparisons between the experimental and theoretical quantities so obtained and also between pairs of theoretical predictions permit an evaluation of properties of mass equations including the quality of extrapolations into regions of unknown nuclei with its inherent difficulties.

Sections 2 and 3 describe experimental and theoretical properties of the energy differences  $\Delta_{T',T}(A)$  and of the symmetry and pairing energies. The theoretical mass predictions are presented in Section 4. Results and the analysis for a set of eleven theoretical mass predictions including the three mentioned above are presented in Section 5 followed by a summary in Section 6.

## 2. Energy differences $\Delta_{T',T}(A)$

Numerous excitation energies of isobaric analog are known experimentally [9]. These energies are related to the ground state energies of neighboring isobaric nuclei. They can therefore also be estimated from the masses of these nuclei by applying corrections due to the differences in Coulomb energies and neutron-proton masses. The above energy differences between isobaric analog states in a given nucleus will be denoted by  $\Delta_{T',T}(A)$  where  $T'$  and  $T$  are, respectively, the isospins of the excited isobaric analog state and the ground state (or a lower lying isobaric analog state). Using this approach, an independent, comprehensive, and global set of energies

$\Delta_{T',T}(A)$  can be deduced from the experimental binding energies or masses [10] of neighboring isobars corrected for the differences in Coulomb energies. General expressions are reported in Ref. [8]. For the special case of  $T' = T + 1$  and  $T_z \geq 0$  one obtains

$$\Delta_{T+1,T}(A) = +M(A, T_z + 1) - M(A, T_z) + \Delta E_C(T_z + 1|T_z, A) - (M_n - M_H). \quad (1)$$

While the energy differences  $\Delta_{T',T}(A)$  are in principle also dependent on  $T_z$ , the  $z$ -component of the isospin  $T$ , the dependence on  $T_z$  is mostly very weak and can be neglected since Coulomb displacement energies  $\Delta E_C(T_z + 1|T_z, A)$  are to a good approximation independent of isospin  $T$  [11].

Theoretically, the energy differences  $\Delta_{T',T}(A)$  between isobaric analog states in the same nucleus are equal to the differences of the respective binding energies (or masses) of these states and hence approximately equal to the differences of the charge-independent parts of the nuclear Hamiltonian. As a consequence

$$\Delta_{T',T}(A) \approx -(E_{\text{sym}}(A, T') + E_{\text{pair}}(A, T')) + (E_{\text{sym}}(A, T) + E_{\text{pair}}(A, T)). \quad (2)$$

It thus follows that the energy differences  $\Delta_{T',T}(A)$  between isobaric analog states can be expressed to a good approximation as differences between symmetry and pairing energies [8].

### 3. Symmetry and pairing energies

Over wide ranges of nuclei the symmetry energies of nuclei can be written as

$$E_{\text{sym}}(A, T) = \frac{a(A, T)}{A} T(T + 1) \quad (3)$$

with approximately constant values for the symmetry-energy coefficients  $a(A, T)$ . Departures from constant values  $a(A, T)$  are observed [8], though. If Eq. (3) is applied to all nuclei, the symmetry energy coefficients  $a(A, T)$  become operationally defined quantities.

Theoretically, Eq. (3) with constant values of  $a(A, T)$  is valid only in an extreme single-particle shell-model approach for nuclei with nucleons in a  $j^n$  configuration with seniority  $v$  and isospin  $T$  as good quantum numbers [12–14]. Approximately constant values of  $a(A, T)$  were found, though, for entire “diagonal” shell regions where neutrons and protons occupy the same major shell-model orbits [15]. It is this property which makes the above symmetry-energy coefficients  $a(A, T)$  useful indicators for departures from shell-model behavior and for the presence of special features as well as (see below) indicators for “non-diagonal” shell regions where valence neutrons and protons occupy different major shell-model regions.

When the effect of pairing in even- $A$  nuclei is included, expressions for the coefficients  $a(A, T)$  and the pairing energies  $P(A, T)$  are easily derived from Eq. (3) and become [8]

$$a(A, T) = \frac{A\Delta_{T+1,T}(A)}{2T + 2} \quad \text{for } A = \text{odd}, \quad (4)$$

$$a(A, T) = \frac{A\Delta_{T+2,T}(A)}{4T + 6} \quad \text{for } A = \text{even or } A = \text{odd}, \quad (5)$$

$$P(A, T) = \frac{1}{4} \left| \frac{2T + 2}{2T + 3} \Delta_{T+2,T+1}(A) - \frac{2T + 4}{2T + 3} \Delta_{T+1,T}(A) \right| \quad \text{for } A = \text{even}. \quad (6)$$

Experimental and theoretical (see below) symmetry energy coefficients  $a(A, T)$  have been obtained from Eq. (5) for both even- $A$  and odd- $A$  nuclei and are displayed in Figs. 1 to 5 for nuclei

with  $T_z \geq 0$ . The experimental values are included in Fig. 1 (see also Fig. 4 in Ref. [8]). Similarly, pairing energies  $P(A, T)$  have been obtained from Eq. (6). They are included in Fig. 6 (see also Fig. 15 in Ref. [8]). Whereas the present results for the experimental values are based on the atomic mass evaluation Ame2003 [10], the earlier ones were based on Ame1995 [16]. Furthermore, the consequences of isospin inversion between the lowest  $T = 0$  and  $T = 1$  states in odd-odd  $T_z = 0$  nuclei was considered by correcting the masses of the respective self-conjugate nuclei between  $A = 34$  and 74. Here, the experimentally established excitation energies  $E_1(T = 0)$  for the first excited  $T = 0$  states compiled in Refs. [9,17] were added to the  $T = 1$  ground-state mass values. Without this correction, the symmetry energy coefficients  $a(A)$  display anomalies. This is seen in Fig. 2 of Ref. [17] because without the above correction the quantity which is displayed becomes

$$a^*(A) = a(A) + \frac{A}{6} E_1(T = 0). \quad (7)$$

As noted earlier [8,17], a few data points in Ame1995 [16] and Ame2003 [10] are estimated mass values based on extrapolations (see Ref. [18], p. 142). Conservative uncertainties were assigned to these values in the mass evaluations, and it was shown that the predicted values are quite reliable within the quoted uncertainties and superior to those from all other currently available mass equations (see p. 1066 and Table I in Ref. [1]). These mass values were included in the present calculations. Error propagation making use of Eqs. (1) and (5) results in uncertainties for the symmetry energy coefficients  $a(A, T)$  which are quite pronounced, as per Eq. (5), for data points with small values of isospin. The uncertainties for  $T = 0$  nuclei in the region below  $A = 100$  which includes estimated mass values will explicitly be shown below.

A detailed analysis of the experimental quantities  $a(A, T)$  and  $P(A, T)$  has been performed previously [8] separately for the diagonal and non-diagonal shell regions labeled by  $(d_i)$  and  $(n_i)$ :

- Region  $(d_1)$  with  $8 \leq N, Z \leq 20$ ,
- Region  $(d_2)$  with  $20 \leq N, Z \leq 28$ ,
- Region  $(d_3)$  with  $28 \leq N, Z \leq 50$ ,
- Region  $(d_4)$  with  $50 \leq N, Z \leq 82$ ,
- Region  $(d_5)$  with  $82 \leq N, Z \leq 126$ ,
- Region  $(n_1)$  with  $8 \leq N \leq 20$  and  $2 \leq Z \leq 8$ ,
- Region  $(n_2)$  with  $20 \leq N \leq 28$  and  $8 \leq Z \leq 20$ ,
- Region  $(n_3)$  with  $28 \leq N \leq 50$  and  $20 \leq Z \leq 28$ ,
- Region  $(n_4)$  with  $50 \leq N \leq 82$  and  $28 \leq Z \leq 50$ ,
- Region  $(n_5)$  with  $82 \leq N \leq 126$  and  $50 \leq Z \leq 82$ ,
- Region  $(n_6)$  with  $126 \leq N$  and  $82 \leq Z \leq 126$ .

It was found that within uncertainties the shell-model dependence  $T(T + 1)$  dominates for the light nuclei in regions  $(d_1)$ ,  $(d_2)$  and  $(d_3)$  with nearly constant values of  $a(A, T)$  as per Eq. (3). An isospin dependence  $T(T + c)$  with  $c > 1$  approaching  $c \approx 4$  prevails for heavy nuclei in regions  $(d_4)$  and  $(d_5)$ .

An interesting situation [17] is present in the *fp*g shell of region  $(d_3)$ . While  $a(A, T)$  is approximately constant over most of the region, a significant increase is observed in the localized region with  $N \approx Z$  and  $76 < A < 96$  indicating a departure from  $T(T + 1)$ . This behavior is apparent

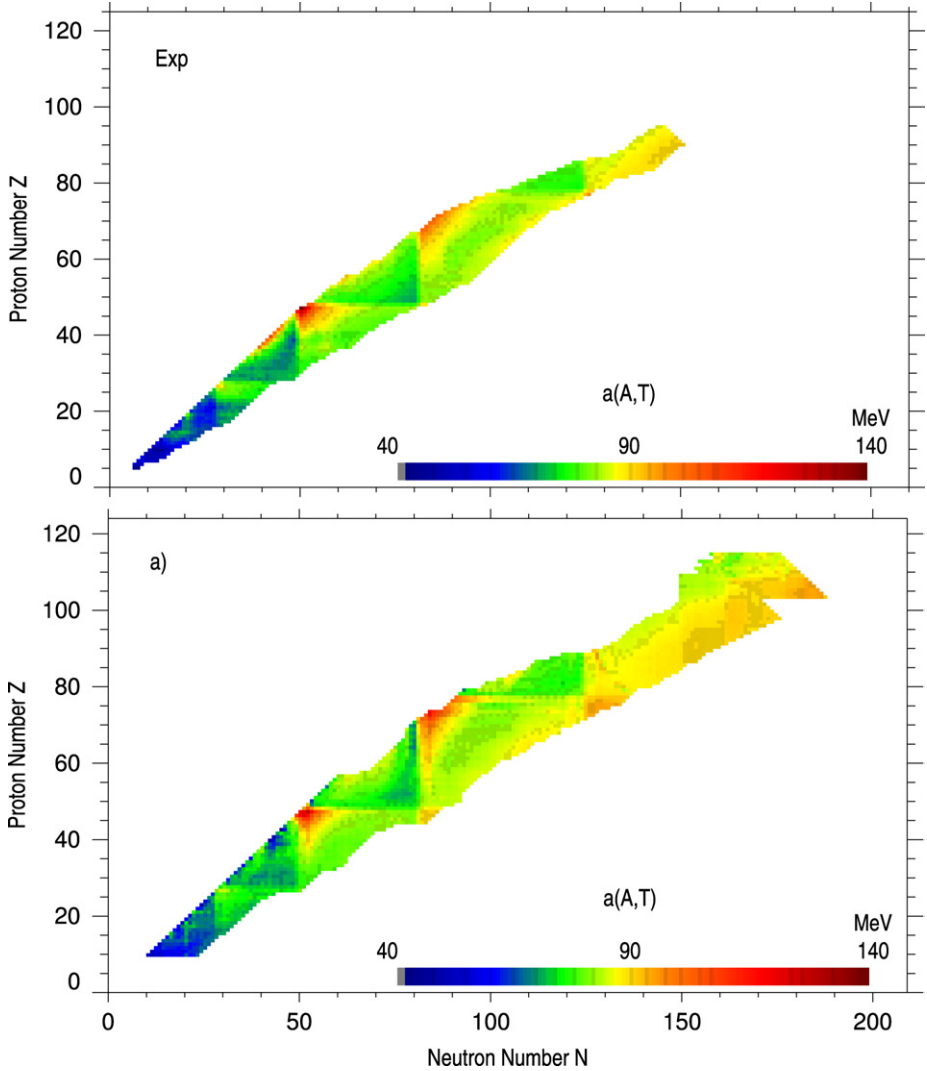


Fig. 1. Symmetry-energy coefficients  $a(A, T)$  as function of neutron and proton numbers  $N$  and  $Z$  (or correspondingly  $A$  and  $T$  with  $T_z \geq 0$ ) deduced from experimental mass data and from the mass equation (a) (see text).

in Fig. 1 from the increased values of the operationally defined quantity  $a(A, T)$  for this range of nuclei. These increased values are in agreement with a dependence on the isospin of the form  $T(T + x)$  with  $x \approx 4$  [17]. This result is compatible with the Wigner supermultiplet model [19].

Major departures from Eq. (3) occur in all “non-diagonal” shell regions where neutrons and protons occupy different major shell-model orbits, particularly for nuclei approaching the  $N = Z$  line. Here, a quantity with the characteristics of a symmetry energy has been derived [8] from an expression for the average neutron-proton interactions leading to an isospin dependence of the symmetry energy given by

$$\tilde{E}_{\text{sym}}(A, T) = \frac{b(A, T)}{A} T(T + c) \quad (8)$$

with  $c > 1$ . Good agreement was observed [8] with constants  $c$  increasing for the regions ( $n_1$ ) to ( $n_5$ ) from  $c \approx 1.6$  to  $c \approx 4.5$ . Systematic effects observed for region ( $n_5$ ) further seem to suggest the need for higher-order correction terms in the number of particles and/or holes.

#### 4. Theoretical mass predictions

The procedures for extracting the energy differences  $\Delta_{T',T}(A)$  between isobaric analog states, the symmetry energies  $E_{\text{sym}}(A, T)$  and symmetry-energy coefficients  $a(A, T)$ , as well as the pairing energies  $P(A, T)$  are identical for experimental mass data and for predicted mass data. Therefore, given identical approaches, the calculation of these quantities for selected mass equations and algorithms for predicting masses of unknown nuclei allows a comparison between the experimental and calculated symmetry energy coefficients  $a(A, T)$  and pairing energies  $P(A, T)$ . This is important since the symmetry energy  $E_{\text{sym}}(A, T)$  provides a signature for the curvature of the mass surface. The quantity  $P(A, T)$ , on the other hand, is an added quantity for calculating masses and therefore less important. While Eqs. (3) and (8) were used in the previous discussion of the experimentally observed symmetry and pairing energies [8], only Eq. (3) with the operationally defined symmetry energy coefficients  $a(A, T)$  will be used in the present work permitting a direct comparison between theoretical and experimental features.

An inspection and evaluation of the above quantities for different mass equations will provide information about the quality and the characteristics of mass equations including the expected characteristics of extrapolations away from the known nuclei.

The following mass equations were selected for this approach, namely

- (a) P. Möller and J.R. Nix, Nuclear mass formula with a finite-range droplet model and a folded-Yukawa single-particle potential (unified macroscopic-microscopic model), 1988; Ref. [20],
- (b) Y. Aboussir, J.M. Pearson, A.K. Dutta and F. Tondeur, Extended Thomas–Fermi method with Strutinski integral (ETFSI), 1992; Ref. [2],
- (c) P. Möller, J.R. Nix, W.D. Myers and W.J. Swiatecki, Droplet model with deformation and microscopic corrections 1995; Ref. [3],
- (d) W.D. Myers and W.J. Swiatecki, Thomas–Fermi model with effective  $\mathcal{N}$ – $\mathcal{N}$  interaction, 1996; Ref. [21],
- (e) J. Duflo and A.P. Zuker, microscopic mass formula with smooth pseudopotential, 10 parameters, 1996; Ref. [5],
- (f) J. Duflo and A.P. Zuker, microscopic mass formula with smooth pseudopotential, 25 parameters, 1995; Ref. [4],
- (g) T. Tachibana, M. Uno, M. Yamada and S. Yamada, Empirical mass formula with proton–neutron interaction, 1988; Ref. [22],
- (h) E. Comay, I. Kelson and A. Zidon, Garvey–Kelson mass predictions by modified ensemble averaging, 1988; Ref. [23],
- (i) J. Jänecke and P.J. Masson, Mass predictions from homogeneous Garvey–Kelson mass relation, 1988; Ref. [24],
- (j) P.J. Masson and J. Jänecke, Inhomogeneous partial difference equations, 1988; Ref. [25],
- (k) L. Satpathy and R.C. Nayak, Infinite nuclear matter model, 1988; Ref. [26].

The above mass equations can approximately be grouped into two classes. The seven equations (a) through (g) constitute equations which are primarily based on  $\mathcal{N}$ – $\mathcal{N}$  interactions with selective macroscopic components from the categories (B), (C) and (D) of Ref. [1]. The four

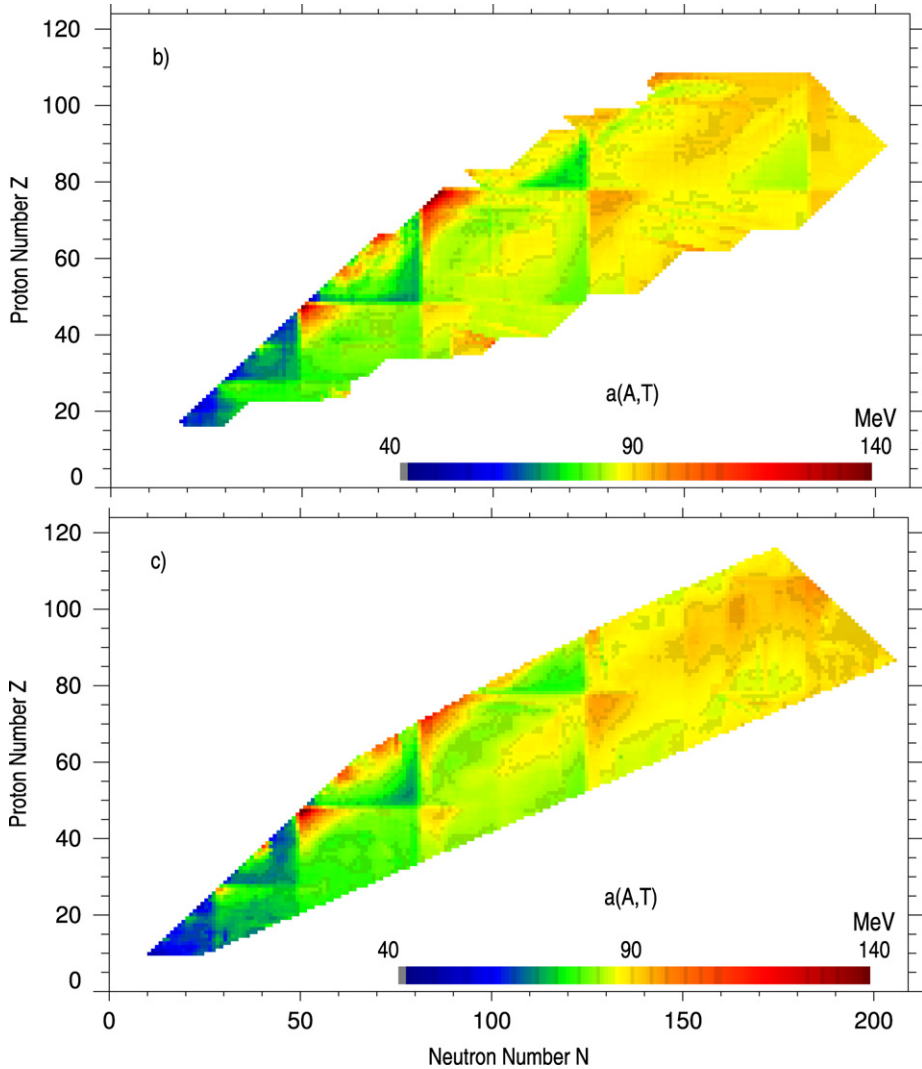


Fig. 2. Symmetry-energy coefficients  $a(A, T)$  as function of neutron and proton numbers  $N$  and  $Z$  (or correspondingly  $A$  and  $T$  with  $T_z \geq 0$ ) deduced from mass equations (b) and (c) (see text).

equations (h) through (k) are primarily based on relations between binding energies or masses of neighboring nuclei belonging to the category (E) of Ref. [1].

The symmetry energy coefficients  $a(A, T)$  obtained from the predictions of the above equations are shown in Figs. 1 to 5 except for equations (e) and (f) which are included instead in Sections 5.2 to 5.6. The coefficients obtained from the experimental data are included in Fig. 1. Similarly, pairing energies  $P(A, T)$  were also obtained and are included together with the experimental pairing energies in Fig. 6. The comparison between the theoretical and experimental quantities  $a(A, T)$  and  $P(A, T)$  is presented and discussed in the following sections. The discussion will concentrate on the implications for the quality and possible shortcomings of the mass equations and algorithms for the prediction of atomic masses. Of particular interest will be

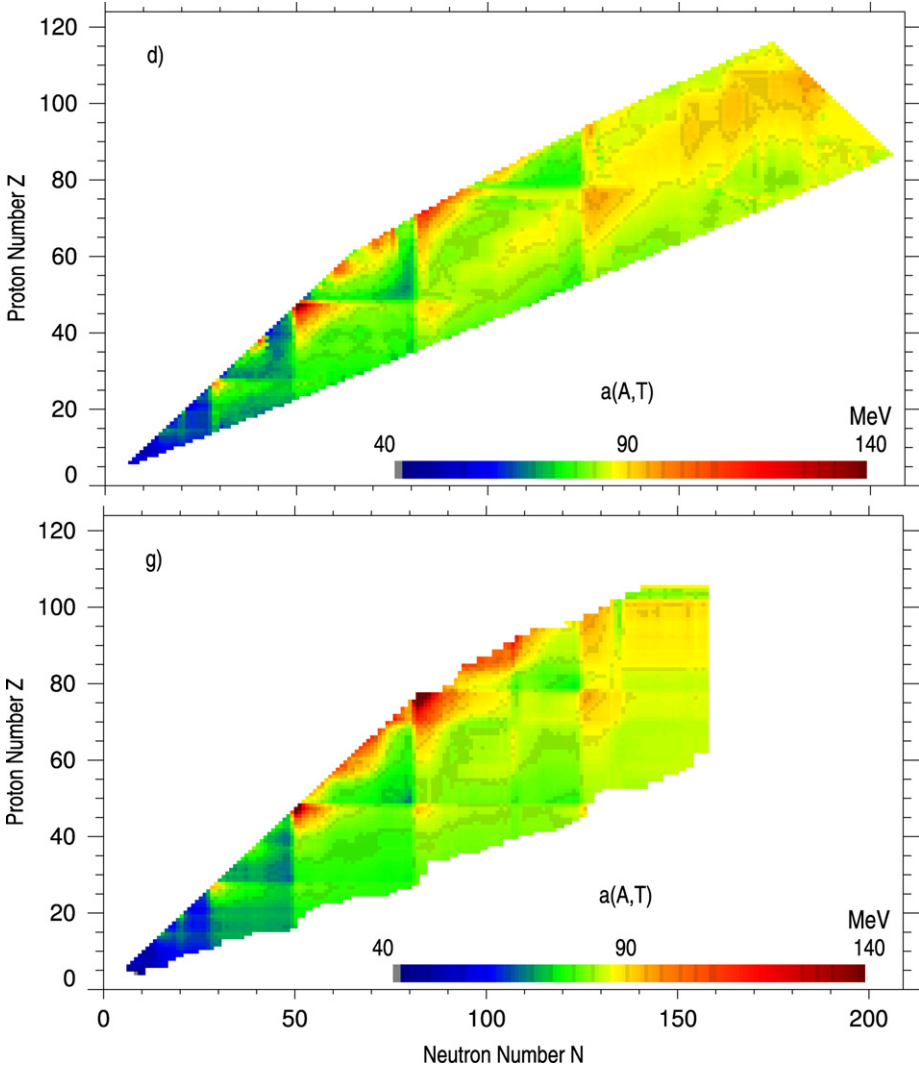


Fig. 3. Symmetry-energy coefficients  $a(A, T)$  as function of neutron and proton numbers  $N$  and  $Z$  (or correspondingly  $A$  and  $T$  with  $T_z \geq 0$ ) deduced from mass equations (d) and (g) (see text).

the identification of regions where disagreements with the experimental results exist as well as regions of extrapolated mass values where the mass equations display different characteristics in the curvature between their predicted mass surfaces.

## 5. Results

### 5.1. Symmetry-energy coefficients $a(A, T)$

As seen in Fig. 1 (see also Fig. 4 in Ref. [8]) the operationally-defined experimental symmetry-energy coefficients  $a(A, T)$  increase from about 40 MeV for the lightest nuclei to about 80 to 90 MeV in the medium-heavy to heavy nuclei. Shell structures result from the dependence of

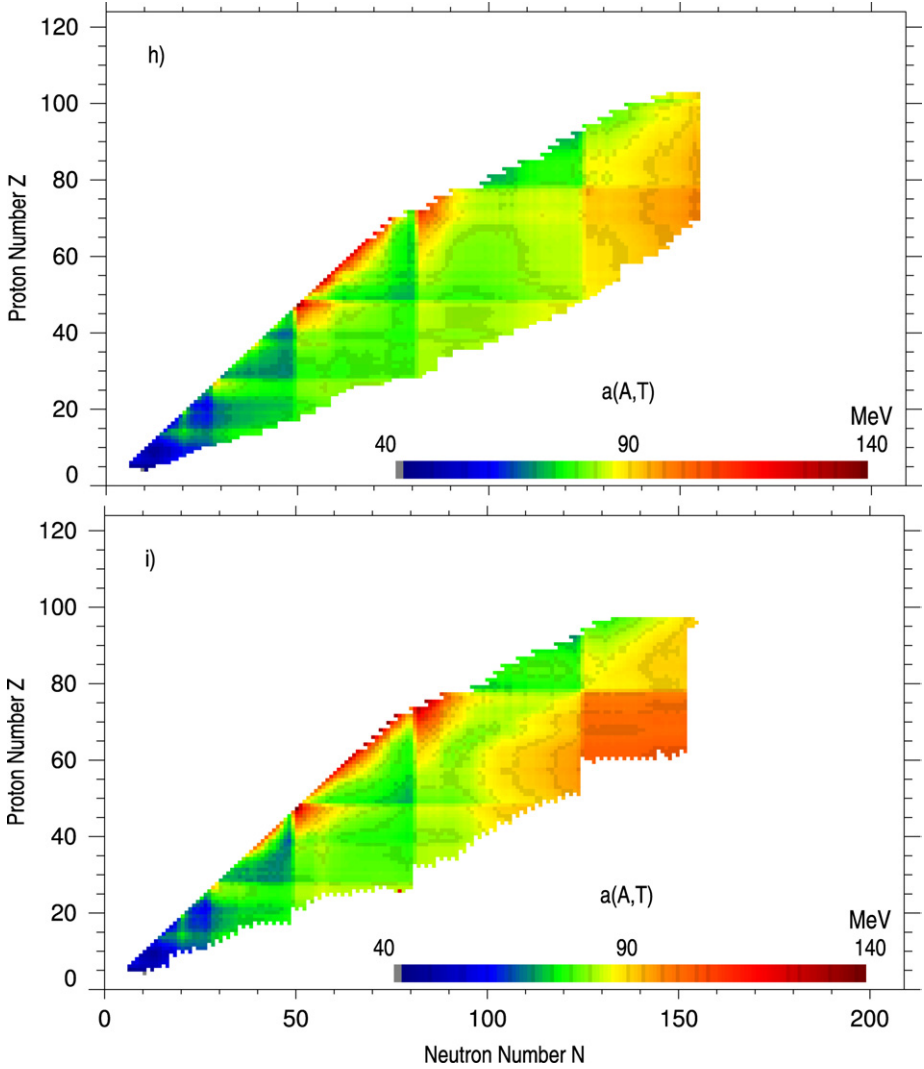


Fig. 4. Symmetry-energy coefficients  $a(A, T)$  as function of neutron and proton numbers  $N$  and  $Z$  (or correspondingly  $A$  and  $T$  with  $T_z \geq 0$ ) deduced from mass equations (h) and (i) (see text).

the symmetry energy on shell-model configurations. Increased values are observed in shell regions where valence neutrons and protons occupy different major shells. This is particularly pronounced for nuclei with only a few particles and/or a few holes in the non-diagonal shell regions ( $n_4$ ) and ( $n_5$ ). Here, the most proton-rich nuclei approach the doubly magic nuclei  $^{100}\text{Sn}$  and  $^{164}\text{Pb}$ . In these non-diagonal shell regions Eq. (3) with constant values of  $a(A, T)$  provides an only approximate representation of the symmetry energy  $E_{\text{sym}}$  [8] because of the observed presence of an increased linear isospin term. Another small region with increased values of  $a(A, T)$  is seen in the diagonal shell region ( $d_3$ ) for nuclei with  $N \approx Z$  centered near  $A \approx 86$ .

The overall characteristics of the coefficients determined from the theoretical equations are shown in the Figs. 1 to 5. As indicated below, the results for equations (e) and (f) are similar to

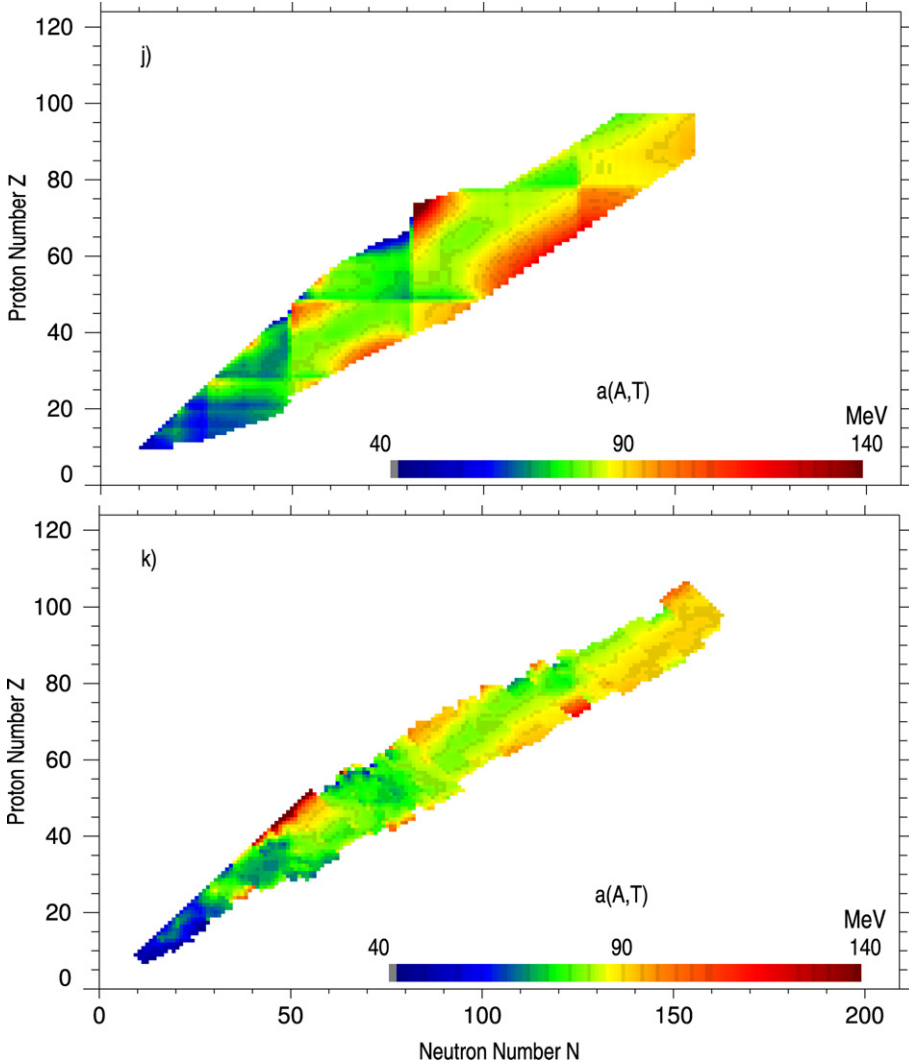


Fig. 5. Symmetry-energy coefficients  $a(A, T)$  as function of neutron and proton numbers  $N$  and  $Z$  (or correspondingly  $A$  and  $T$  with  $T_z \geq 0$ ) deduced from mass equations (j) and (k) (see text).

those for equations (g) and (h). All coefficients are reasonably similar to those of the experimental coefficients, but important differences are also present. The increase from the light to the heavy nuclei is observed. A dependence of the symmetry energy on shell structures, particularly in the most proton-rich heavier nuclei beyond  $N, Z = 28$ , is seen for almost all equations.

The presence of the increased experimental values of  $a(A, T)$  for nuclei in the diagonal region ( $d_3$ ) for nuclei close to  $N = Z$  is not reproduced except for a single theoretical prediction.

In region ( $d_4$ ) the experimental results shown in Fig. 1 also seem to display an increase towards the  $N = Z$  line. Results at and very close to  $N = Z$  are missing, though. However, as was shown earlier [8], the coefficients  $a(A, T)$  in this region display a dependence on isospin as  $T(T+x)$  with  $x > 1$  over the entire shell region, which appears to explain the observed characteristics.

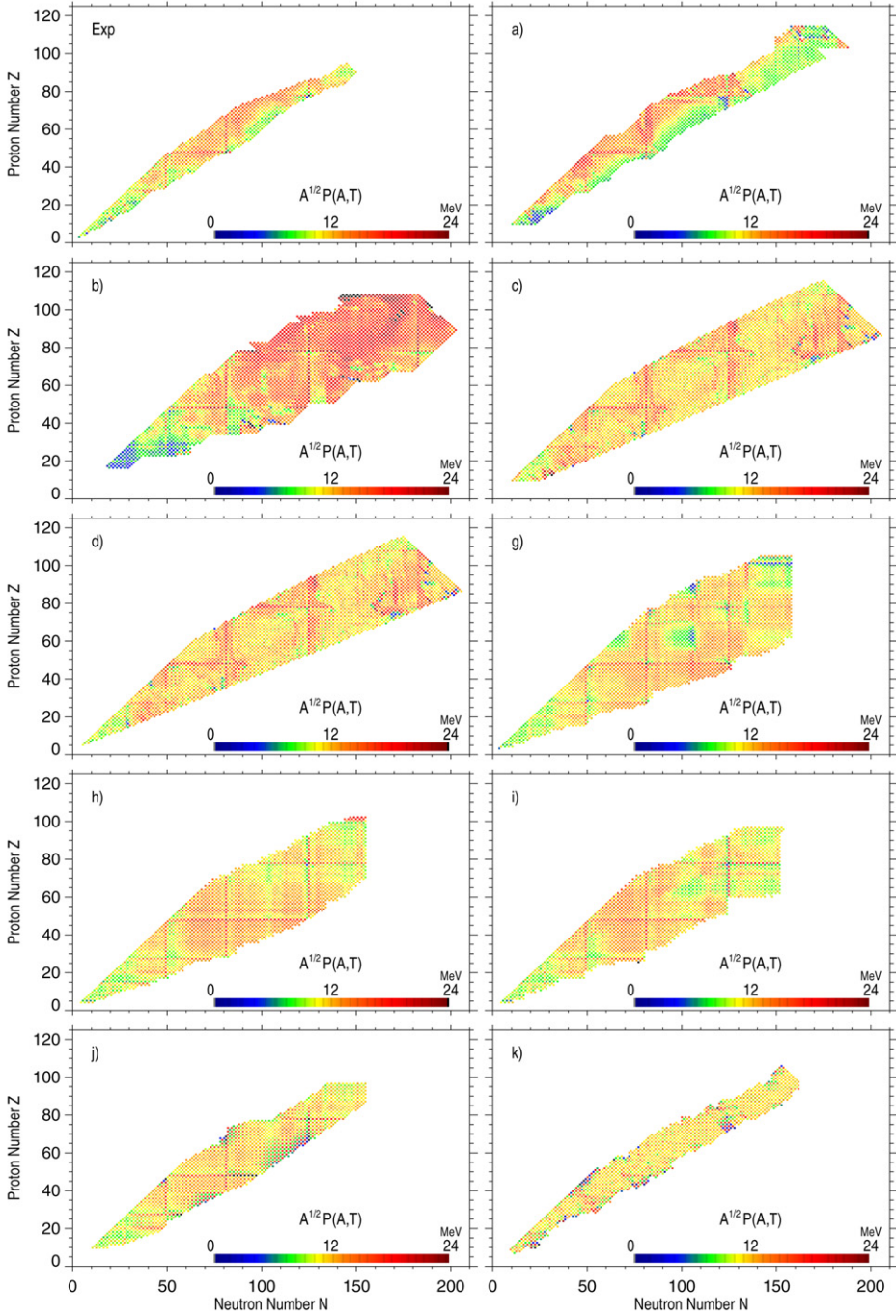


Fig. 6. Pairing energies  $P(A, T)$  (multiplied by the square root of  $A$ ) as function of neutron and proton numbers  $N$  and  $Z$  (or correspondingly  $A$  and  $T$  with  $T_z \geq 0$ ) deduced from experimental mass data and from mass equations or algorithms. The enhanced values for nuclei with magic neutron or proton numbers reflect upon discontinuities in the symmetry energies and are unrelated to pairing (see text).

This is different from the behavior seen in region ( $d_3$ ) with the essentially constant values of  $a(A, T)$  over most of the region except for the rapid increase for nuclei approaching  $N = Z$ . However, several of the theoretical predictions for region ( $d_4$ ) show in addition a very pronounced strong increase for the symmetry energy coefficient  $a(A, T)$  near  $N \approx Z$  far exceeding the slight experimentally observed increase for the entire region. Equations (g), (h) and (i) display this increase for a wide range of mass values  $A$  centered at about  $A \approx 128$ . Equations (b), (c) and (d) show a similar behavior, but the region of increased values is split into two smaller regions centered at about  $A \approx 122$  and  $A \approx 140$ .

In the diagonal shell region ( $d_5$ ) a few mass predictions for proton-rich nuclei reach close to the  $N = Z$  line. Here, equation (g) shows again increased values of  $a(A, T)$  for the most proton-rich nuclei, but some of these nuclei are not expected to be particle stable (see e.g. Fig. 4 in Ref. [1]).

Equation (j) exhibits strong departures from the experimental and the other theoretical values for the most proton-rich and the most neutron-rich nuclei. This is seen over small regions of the very proton-rich nuclei with  $N \leq 50$  and  $Z \geq 50$  where the values for  $a(A, T)$  appear to be too small. An even more pronounced effect is seen for the most proton-rich nuclei below and above  $N = 82$  where  $a(A, T)$  appears to be too small and too big, respectively. For the very neutron-rich nuclei major problems also appear to be present over wide ranges of mass values in the middle of non-diagonal shell regions, particularly for  $A = 90$  to 125 and for  $A = 145$  to 220. Here, the quantity  $a(A, T)$  appears to be systematically too big.

Equation (k) does not display shell effects. Some problems for proton- and neutron-rich nuclei are also present, particularly for the proton-rich nuclei near  $N = Z$  above  $A = 80$ .

A significantly enhanced sensitivity to compare the theoretical symmetry energy coefficients  $a(A, T)$  with the experimental quantities and with each other is possible by inspecting the individual differences of the quantities  $a(A, T)$ . This provides a sensitive test for the goodness of the curvature of the nuclear mass surface. The residuals over the region of known experimental data have been obtained but these figures are not shown here. All residuals display departures from the experimental values. The most pronounced departures are the results for region ( $d_3$ ) near the  $N = Z$  line, but smaller differences were also observed in other experimental regions.

Similarly, comparisons between the symmetry energy coefficients  $a(A, T)$  extracted for pairs of the various theoretical mass predictions have also been obtained (not shown) because overall agreement or perhaps disagreement particularly in extrapolated regions far from the line of  $\beta$ -stability may provide further insight. Departures were indeed observed between all equations except between equations (c) and (d) which (except for the very light nuclei) are based on the same analytical expression with only slightly different coefficients. This is also seen directly from Figs. 2 and 3.

Instead of displaying the above residuals, it was concluded that a clearer and more direct understanding of the observed effects can be obtained by displaying and comparing the coefficients  $a(A, T)$  for a few selected chains of nuclei separately for the experimental and the predicted values for all equations (a) through (k). This is discussed in the following subsections for nuclei with  $T = 0$  and for nuclei with  $A = 100, 132, 164$  and 208. The latter  $A$ -chains intersect the middle of the shell regions ( $n_4$ ), ( $d_5$ ), ( $n_5$ ) and ( $d_5$ ).

## 5.2. Nuclei with $T = 0$

As mentioned, the most pronounced discrepancies between the theoretically predicted and the experimental symmetry energy coefficients  $a(A, T)$  occur at and near  $T = 0$  in the diagonal

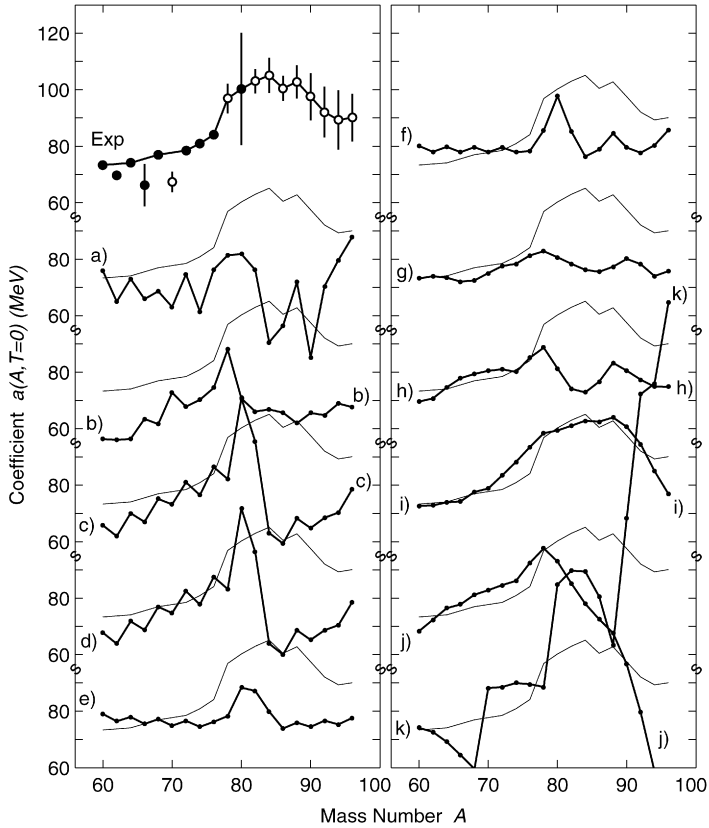


Fig. 7. Experimental (top) and eleven calculated symmetry energy coefficients  $a(A, T = 0)$  for nuclei with  $T = 0$  as function of mass number  $A$  in the  $fp_g$ -shell ( $d_3$ ). Experimental data points are shown as filled circles. Open circles denote data points derived from a combination of experimental and predicted masses (see text) or from predicted masses only ( $A = 84, 92, 94$ ). Uncertainties are shown if  $> 0.7$  MeV. All values are connected by straight solid lines with the exception of the data points for  $A = 62, 66$  and  $70$  (see text). The values derived from the mass equations are displaced vertically by 40 MeV each and are also connected by straight solid lines. In addition, for comparison, the results from the experimental values are overlaid without uncertainties with the calculated values as thin lines.

region ( $d_3$ ) below  $A = 100$ . This is the region of nuclei which has been discussed previously in terms of mixing of correlated  $T = 0$  and  $T = 1$   $n-p$  pairs [17].

Fig. 7 displays the coefficients  $a(A, T = 0)$  for nuclei with  $T = 0$  over the range  $A = 60$  to 96 for both, the experimental data as well as all eleven theoretical predictions. The first graph in the figure shows the experimental values including uncertainties deduced from the atomic mass evaluation Ame2003 [10]. Some data points (open circles), as mentioned, are obtained with the inclusion of predicted mass values. A significant increase of the experimental coefficients by over 30 MeV in this shell region centered near  $A \approx 86$  is seen relative to a value of  $a(A, T) \approx 70$  MeV. Such a value is expected, as explained previously [8], if the shell-model dependence  $T(T + 1)$  observed over most of the shell region ( $d_3$ ) were to extend to the  $T = 0$  line.

The graph for the experimental results is very similar to that shown in Fig. 2 of Ref. [17]. It differs from the one shown before primarily because the ground state masses for isospin inverted odd-odd selfconjugate nuclei with  $T = 1$  ground states were corrected for the experimentally

observed excitation energies  $E_1(T = 0)$  of the energetically lowest  $T = 0$  state. As a result the value for  $A = 74$  follows the smooth dependence on  $A$  very closely. The low values seen for  $A = 62, 66$  and  $70$  may suggest the need for revised ground state mass values and/or the existence of  $T = 0$  states at a lower excitation energy than so far reported.

The experimental data points are connected by straight lines with the exception of the low values. These lines are repeated and overlaid for all theoretical results to permit a simple comparison.

Essentially all predicted coefficients  $a(A, T = 0)$  show major departures from the experimentally observed values, particularly for high mass numbers  $A$ . This includes the results from equations (a) through (g) which are primarily based on  $\mathcal{N}$ - $\mathcal{N}$  interactions. Equations (c) through (g) describe the observed behavior for values of low  $A$  reasonably well, but equations (a) and particularly (b) are low in this region. None of the results for equations (a) through (g) display any similarity to the experimental values at higher values of  $A$  with the broad maximum at  $A \approx 86$ . Instead, they display very low values beyond  $A \approx 80$  which is particularly drastic for equations (a), (b), (c) and (d). Some oscillatory structure is seen for equations (a) through (d) possibly suggesting isospin inversion with predicted  $T = 1$  ground states for nuclei with  $A = 4n + 2$ .

The four equations (h) through (k) which are based on binding energy relations show different characteristics. Surprisingly, equation (i) displays almost perfect agreement with the experimental values. This can also be seen by comparing Figs. 1 and 4. The results for equation (h) have some similarity to those from equation (g) but differ greatly from those of equation (i) even though both, (h) and (i), are based on the same physical background [27–29]. The results for equations (j) and (k), finally, demonstrate rather serious problems at high mass numbers of  $A > 80$  which are far outside acceptable values.

A similar figure for the coefficients  $a(A, T)$  for all  $T = 0$  states with mass values below  $A = 56$  was also obtained but is not shown here. It was observed that despite some scattering of the data points, the experimental and all predicted values are reasonably similar and do not display major differences.

### 5.3. Nuclei with $A = 100$

The coefficients  $a(A = 100, T)$  for the nuclei with  $A = 100$  beginning at the nucleus  $^{100}\text{Sn}$  intersect the middle of the non-diagonal shell region ( $n_4$ ). Since Eq. (3) with constant  $a(A, T)$  is not a good approximation in non-diagonal shell regions [8], the operationally defined  $a(A, T)$  display very large values for nuclei with small  $T$ . Here, the number of neutron-particles and proton-holes is small. Fig. 8 displays the values  $a(A = 100, T)$  obtained from the experimental mass data and from all eleven mass equations but only for small values  $T$  from 0 to 4. Fig. 9 continues the display with a small overlap for all values  $T \geq 3$ . Here, the experimental values are again repeated and overlaid with the calculated values for comparison.

The strong increase of the values  $a(A = 100, T)$  approaching  $T = 0$  as result of the increased linear isospin term in this non-diagonal shell region is seen in Fig. 8 for the experimental values and for most equations. Only equations (a) and particularly (j) significantly underestimate the observed increase towards  $T = 0$ . Fig. 9 shows for larger values of  $T$  the continued decrease of the experimental values which is also seen for all equations with mostly very good agreement, followed by rather flat structures for several of the equations. Equation (b) suggests a shell transition near  $T \approx 10$  or  $Z \approx 40$  not observed experimentally. Similar but much weaker such effects are also seen for equations (c) and (d). The decrease seen for equation (d) beyond  $T = 13$  is stronger than for most other equations suggesting a change in the linear isospin term. Equations (j) and (k)

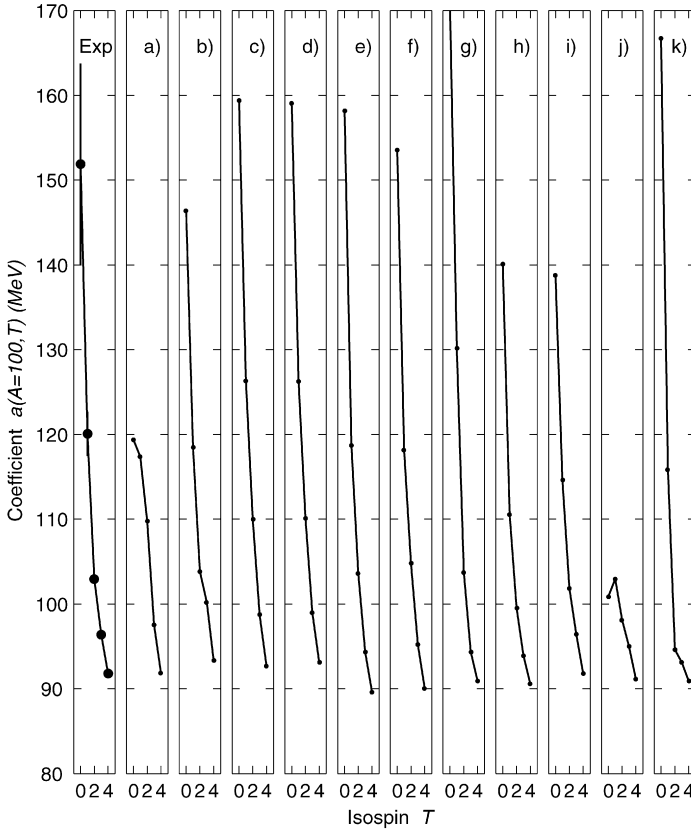


Fig. 8. Experimental (left) and eleven calculated symmetry energy coefficients  $a(A = 100, T)$  for nuclei with  $A = 100$  as function of isospin  $T$  for  $T = 0$  to 4. Experimental data points are shown as filled circles. Uncertainties are shown if  $> 0.7$  MeV. These values are connected by straight solid lines. The values derived from the mass equations are displaced horizontally and are also connected by straight solid lines.

show strong increases beyond  $T = 18$ , and particularly the increase for equation (j) is far outside acceptable values.

For equations (e) through (i) the reported range extends across the magic proton number  $Z = 28$  at  $T = 22$ . The predicted increases from  $T = 20$  to 22, smaller though for equation (g), are likely due to the transition into a different shell region.

It is not quite clear which equations are likely to provide the best extrapolations to very neutron-rich nuclei, but equations (c) and (e) through (i) appear favored.

#### 5.4. Nuclei with $A = 132$

The coefficients  $a(A = 132, T)$  for the nuclei with  $A = 132$  intersect the diagonal shell region ( $d_4$ ) and reach the doubly-magic nucleus  $\text{Sn}^{132}$  at  $T = 16$ . Note that the transition into the next shell region stretches over two steps from  $T = 14$  to 16 because of the way the symmetry energy coefficient  $a(A, T)$  is constructed as per Eq. (5). The values then extend into the non-diagonal shell region with  $82 \leq N \leq 126$  and  $28 \leq Z \leq 50$ . The results for the experimental and predicted values are shown in Fig. 10. Even though the initial shell region ( $d_4$ ) encompasses a diagonal

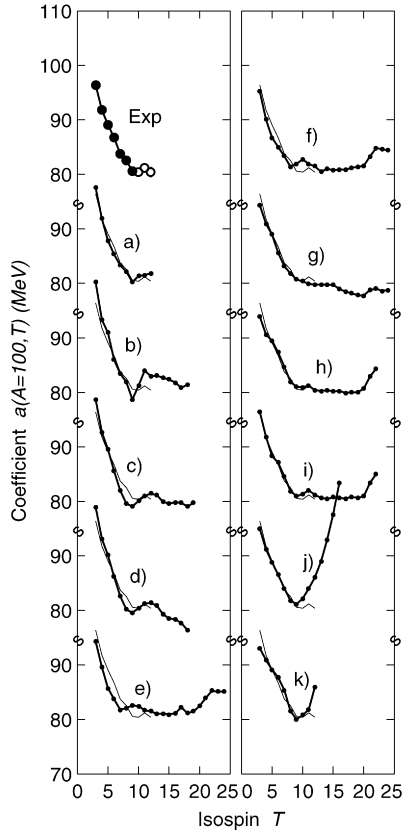


Fig. 9. Experimental (top) and eleven calculated symmetry energy coefficients  $a(A = 100, T)$  for nuclei with  $A = 100$  as function of isospin  $T$  for  $T \geq 3$ . Experimental data points are shown as filled and open circles. Uncertainties are shown if  $> 0.7$  MeV. These values are connected by straight solid lines. The values derived from the mass equations are displaced vertically by 20 MeV each and are also connected by straight solid lines. In addition, for comparison, the results from the experimental values are overlaid with the calculated values as thin lines.

shell with neutrons and protons occupying the same major shell-model orbits, the coefficients  $a(A, T)$  are not constant. They decrease with neutron excess because, as was found earlier [8], the symmetry energy depends on isospin as  $T(T + x)$  with  $x > 1$  over the entire shell region. This decrease is reproduced by most mass equations with the best agreement seen for equations (h) and (i). Small positive and negative differences between calculated and experimental values are seen for equations (a) through (g), and larger ones for (j) and (k).

An interesting phenomenon is observed for very small values of  $T$  for equations (f) through (i), particularly (h) and (i). Here, a significant increase of  $a(A = 132, T)$  is seen for  $T \leq 3$  when approaching  $T = 0$ , similar to the effect observed in region ( $d_3$ ) for the experimental data and for equation (i). The strong increase towards  $T = 0$  is already seen particularly in Fig. 4 and mentioned in Section 5.1. This behavior may have similar origin. The mass value  $A = 132$  used for Fig. 10 is close to the maximum of this effect at  $A \approx 128$  mentioned there. It was also suggested from Figs. 2 and 3 that for equations (b), (c) and (d) the predicted effect is split into two smaller regions centered at  $A \approx 122$  and  $A \approx 140$ . The value  $A = 132$  used in Fig. 10 is in the middle between these values which seems to explain the predicted drop towards

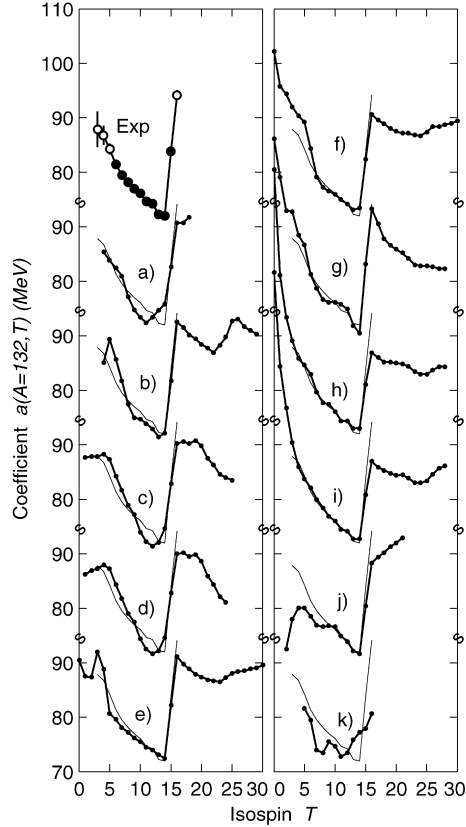


Fig. 10. Experimental (top) and eleven calculated symmetry energy coefficients  $a(A = 132, T)$  for nuclei with  $A = 132$  as function of isospin  $T$  for  $T \geq 0$ . Experimental data points are shown as filled and open circles. Uncertainties are shown if  $> 0.7$  MeV. These values are connected by straight solid lines. The values derived from the mass equations are displaced vertically by 20 MeV each and are also connected by straight solid lines. In addition, for comparison, the results from the experimental values are overlaid with the calculated values as thin lines.

$T = 0$ . It should be noted, though, that nuclei with  $T \leq 1$  are likely to be particle unstable for  $A = 132$  (see e.g. Ref. [30]).

The observed increase in the symmetry energy coefficient at the crossing into a new major shell region at the doubly magic nucleus  $^{132}\text{Sn}$  with  $T = 14$  to 16 is well reproduced only for equations (b) and (g). Reduced steps are seen for essentially all other equations. The shell step is not seen for equation (k).

No experimental data exist beyond  $^{132}\text{Sn}$ . The predicted characteristics in the region of more neutron-rich nuclei do not display a consistent pattern except that the results for the pairs of equations (c) and (d), (e) and (f), (h) and (i) are similar. Equations (a) and (j) display an increase beyond the shell crossing which is particularly questionable for equation (j). A strong unexplained increase beyond  $T = 23$  is seen for equation (b) and weaker ones for equations (e), (f), (h), and (i).

The comparison of the results for all equations at and beyond the shell crossing at  $^{132}\text{Sn}$  does not provide a consistent behavior. Only equations (b) and (g) reproduce the full shell step of the symmetry energy coefficient, and an inconsistent behavior beyond the crossing is indicated. It

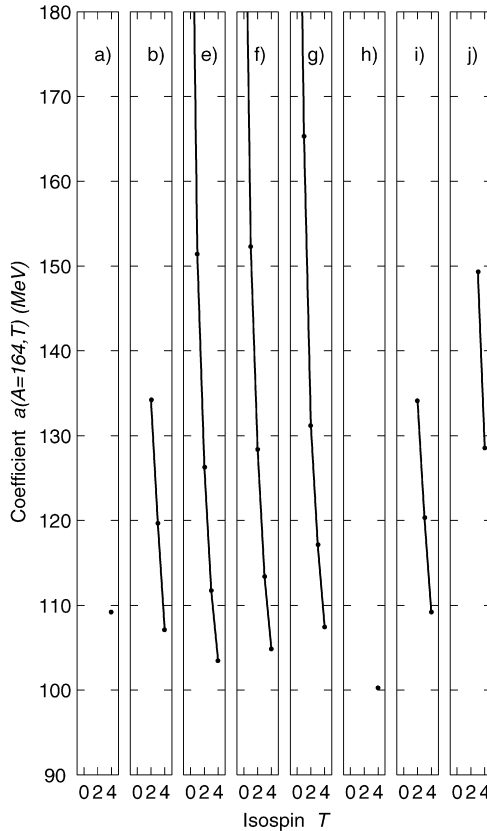


Fig. 11. Available calculated symmetry energy coefficients  $a(A = 164, T)$  for nuclei with  $A = 164$  as function of isospin  $T$  for  $T = 0$  to 4. No experimental values are available. The values derived from the mass equations are displaced horizontally and are connected by straight solid lines.

is not clear which characteristics will prevail for the actual nuclei even when the predictions are compared to the behavior in other shell regions including  $A = 208$  (see below). Equations (e) and (f) are possibly favored.

### 5.5. Nuclei with $A = 164$

The coefficients  $a(A = 164, T)$  for the nuclei with  $A = 164$  beginning at the particle unstable nucleus  $^{164}\text{Pb}$  intersect the middle of the non-diagonal shell region ( $n_5$ ). Figs. 11 and 12 display the results. The behavior should be similar to that described above for  $A = 100$  and in fact it is. Here again, a strong increase towards small values of  $T$  approaching  $T = 0$  is expected due to the fact that the linear isospin term in this shell region is greater than unity and the number of neutron-particles and proton-holes is small. This increase is seen in Fig. 11 for the available data. It should be noted, though, that nuclei up to  $T \approx 3$  are expected to be particle unstable (see e.g. the results for equation (i) in Fig. 4 or Ref. [30]).

The continued decrease with increasing  $T$  is seen for the experimental results in Fig. 12 up to  $T \approx 13$ . At this value of  $T$  a relatively sharp unexplained minimum is observed, reproduced only

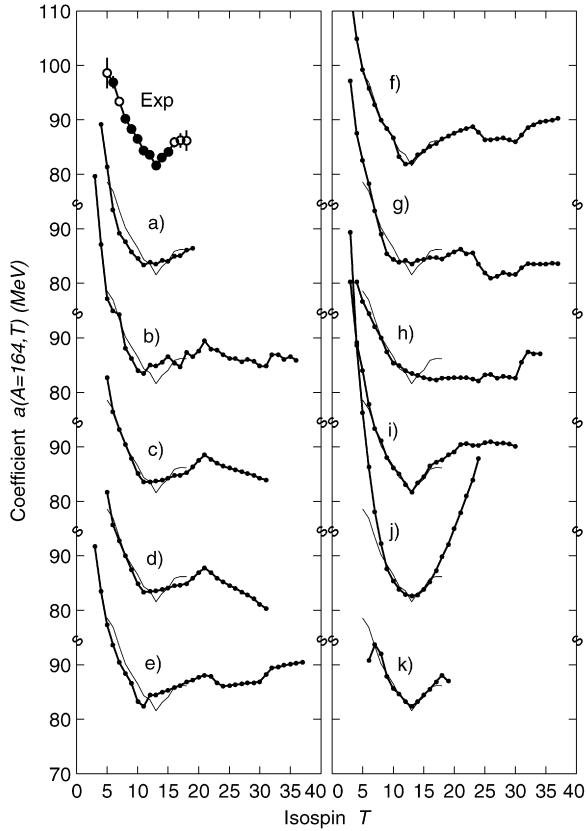


Fig. 12. Experimental (top) and eleven calculated symmetry energy coefficients  $a(A = 164, T)$  for nuclei with  $A = 164$  as function of isospin  $T$  for  $T \geq 3$ . Experimental data points are shown as filled and open circles. Uncertainties are shown if  $> 0.7$  MeV. These values are connected by straight solid lines. The values derived from the mass equations are displaced vertically by 20 MeV each and are also connected by straight solid lines. In addition, for comparison, the results from the experimental values are overlaid with the calculated values as thin lines.

by equations (f), (i), (j) and (k), and also less pronounced for the other equations. This minimum is part of a broad band with low values of  $a(A, T)$  seen in Figs. 1 to 5 for the experimental results and most equations stretching across the entire non-diagonal shell region ( $n_5$ ) of deformed nuclei from  $N = 82$  to  $Z = 82$ .

Several of the calculated results also display a weak maximum near  $T \approx 22$  of unknown origin followed by more constant or mostly decreasing values. The increase for equation (j) is much too strong to be acceptable. Increased values for equations (b) and (e) through (h) at  $T = 30$  to  $32$  are likely due to the shell crossing at  $Z = 50$ , strongest for equation (h).

The predicted characteristics for large neutron excess do again not show a consistent behavior. The comparison of the results for all equations may suggest that the most realistic behavior is one with a rather flat possibly slightly increasing slope as given by equations (b), (c), (e), (f), or (g).

### 5.6. Nuclei with $A = 208$

The coefficients  $a(A = 208, T)$  for the nuclei with  $A = 208$  intersect the diagonal shell region ( $d_5$ ) and reach the doubly-magic nucleus  $^{208}\text{Pb}$  at  $T = 22$ . The expected behavior for this

value of  $A$  as displayed in Fig. 13 is similar to that described above in Fig. 10 for  $A = 132$  where the corresponding transition into the diagonal shell region with  $N \geq 126$  and  $50 \leq Z \leq 82$  occurs at  $^{132}\text{Sn}$  with  $T = 16$

As for  $A = 132$  the values of  $a(A = 208, T)$  in this shell are not constant but decrease with  $A$  both for the experimental results and for most theoretical predictions. This indicates departures from the simple  $T(T + 1)$  dependence on isospin  $T$  with an increased linear isospin term (see Ref. [8]). Best agreement is seen for equations (c) through (g), and also over the limited range of experimental results for equations (h), (i) and (j). It should be noted, though, that nuclei up to  $T = 10$  or 11 are expected to be particle unstable (see e.g. the results for equation (i) in Fig. 4 or Ref. [30]).

All equations except (k) reproduce the increase in the symmetry energy coefficient at the transition into the non-diagonal shell region at  $^{208}\text{Pb}$  very well. This is different from the situation for  $A = 132$  where only two equations reproduce the full shell step seen experimentally. Equation (a) and to a lesser extent (c) and (d), have the step somewhat averaged out.

No experimental data exist beyond the major shell break. An initial decrease is observed for equations (b) through (h) which seems to represent a realistic behavior except that the slopes differ considerably especially for equation (d). The increases seen for (i) and particularly (j) appear unrealistic. Beyond  $T \approx 30$  some of the equations show a flattening out and even increasing values of  $a(A = 208, T)$ . It is thus apparent that the predictions for very neutron-rich nuclei do again not exhibit a consistent pattern.

### 5.7. Pairing energies

The quantities displayed in Fig. 6 will be used exclusively for the discussion of the characteristics of the pairing energies  $P(A, T)$ . The figure displays  $\sqrt{A}P(A, T)$ , the pairing energies as defined in Eq. (6) multiplied by a factor which accounts for the overall decrease with mass number  $A$ . The quantity  $\sqrt{A}P(A, T)$  is shown for the theoretical approaches together with those for the experimental values. This makes it possible to compare the theoretically predicted and the experimental pairing energies. While in reasonable overall agreement, differences are also seen.

As noted earlier [8], the experimental values for  $\sqrt{A}P(A, T)$  are approximately constant and on the order of 12 MeV. Increased pairing of the experimental values and theoretical predictions appears to be present, though, for nuclei with magic neutron and proton numbers, even enhanced for doubly magic nuclei. However, these increased values are *not* due to pairing but instead they are due to the discontinuities of the symmetry energies at shell crossings. Eq. (6) for  $P(A, T)$  assumes only weak changes in the symmetry energy above and below the selected nucleus such that the contributions from the symmetry energy cancel in the difference expression. This is not the case at shell crossings when discontinuities are present as shown above. The observed increased values for  $P(A, T)$  can in principle be used to obtain information about these discontinuities.

In the regions away from magic neutron and proton numbers decreased pairing is observed experimentally for deformed nuclei, particularly in region ( $n_5$ ). Predictions differ in these regions. Only the pairing energies for equation (a) show the experimentally observed reduced pairing in region ( $n_5$ ) for deformed nuclei and some indication is also seen for equations (g) and (i). Essentially all other equations show mostly constant values of  $\sqrt{A}P(A, T) \approx 12$  MeV. For equation (b) much increased pairing is predicted for all nuclei above  $A \approx 170$  contrary to the experimental results. Strongly reduced pairing is seen for equation (j) for certain proton-rich and neutron-rich nuclei where the coefficient  $a(A, T)$  is also problematic, and no shell-related pairing is observed for equation (k).

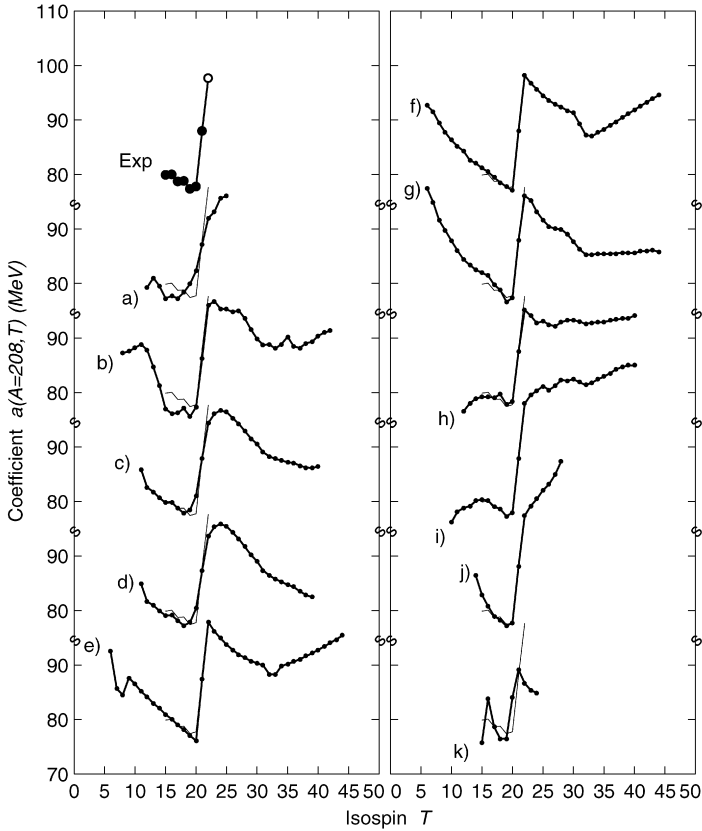


Fig. 13. Experimental (top) and eleven calculated symmetry energy coefficients  $a(A = 208, T)$  for nuclei with  $A = 208$  as function of isospin  $T$ . Experimental data points are shown as filled and open circles. Uncertainties are shown if  $> 0.7$  MeV. These values are connected by straight solid lines. The values derived from the mass equations are displaced vertically by 20 MeV each and are also connected by straight solid lines. In addition, for comparison, the results from the experimental values are overlaid with the calculated values as thin lines.

## 6. Discussion

### 6.1. General predictions

The predictions from the mass equations (a) through (g) are primarily based on  $\mathcal{N}-\mathcal{N}$  interactions with selective macroscopic components as noted earlier. Properties and phenomena related to these and other equations and algorithms have been discussed in great detail by Lunnay et al. [1].

The coefficients  $a(A, T)$  obtained from these equations agree reasonably well with the experimental coefficients over the region of known nuclei. This can be seen from Figs. 8 through 13. However, a serious problem exists for nuclei at and near  $T = 0$  in the diagonal shell region ( $d_3$ ) as seen in Fig. 7. The predicted values display an irregular behavior particularly beyond  $A \approx 80$ . None of the equations reproduce the broad bump observed and centered near  $A = 86$ . This may be important for predictions related to the astrophysical rp-process.

The characteristics for extrapolations of equations (a) through (g) into the region of neutron-rich nuclei can be seen in Figs. 9, 10, 12, and 13. A more regular pattern is observed compared to that for  $T = 0$  nuclei. However, there exist also departures from smooth structures as well as significant differences in the trends for the predicted values of  $a(A, T)$ . This consequently affects the curvature of the nuclear mass surface. Even the mass equations (c), (d), (e) and (f) of Refs. [2–5], which are currently believed to provide the most reliable extrapolations, show this effect. This could therefore influence predictions related to the astrophysical  $r$ -process. Here, long-range extrapolations are required into regions of very neutron-rich nuclei particularly with  $100 < A < 125$  and  $A > 150$  (see e.g. Ref. [30]).

Equations (h) through (k) are multi-parameter equations based primarily on relations between binding energies or masses of neighboring nuclei. The underlying physical concepts in the derivation of these equations are important and have also been discussed by Lunney et al. [1].

Not all multi-parameter equations reproduce the coefficients  $a(A, T)$  well over the range of known nuclei as can be seen in Figs. 8 through 13. Whereas equations (h) and (i) provide good and occasionally excellent agreement, equations (j) and (k) are seemingly problematic. The most significant discrepancy for essentially all mass equations (see Fig. 7) is the fact that only the predictions from the multi-parameter equation (i) reproduce the increased values for  $a(A, T)$  observed for nuclei with  $T = 0$  and nearby in the  $fp$ -shell ( $d_3$ ) below  $A = 100$ . The difference between equations (h) and (i) is surprising since both are based on the same underlying principles (see below). The observed behavior appears to be related to the Wigner energy.

The characteristics of extrapolations for equations (h) through (k) into the regions of very neutron-rich nuclei can again be seen from Figs. 9, 10, 12 and 13. Equations (h) and (i) provide characteristics similar to the equations (a) through (g) except possibly for equations (i) in the heavier nuclei beyond  $A \approx 180$ . Predictions from equations (j) and (k) should not be considered.

## 6.2. Special effects

The behavior of the symmetry energy coefficients  $a(A, T)$  for nuclei with  $N \approx Z$  in region ( $d_3$ ) encompassing the upper  $fp$ -shell requires special attention. The effects is centered near  $A \approx 86$  in a region which is dominated by  $1g_{9/2}$  shell-model orbits [17]. It can be seen for even- $A$  and odd- $A$  nuclei with  $T \leq 2$ . Here, the so-called Wigner energy plays a special role. A Wigner term was originally introduced [31,32] to phenomenologically describe a cusp in the nuclear mass surface for  $N = Z$  necessitating a term linear in  $|N - Z|$ . Since liquid drop models and mean field theories do not account for such a term, various slightly different expressions were introduced. The name results from the fact that the Wigner supermultiplet model [19] based on  $SU(4)$  spin-isospin symmetry contains a symmetry energy term  $E_{\text{sym}}$  proportional to  $T(T + 4)$  and hence generates a cusp at  $T = 0$ .

The parameterization used in the present work is based on the shell-model expression of Eq. (3) where  $E_{\text{sym}}$  is proportional to  $T(T + 1)$  (with constant values of  $a(A, T)$ ). This symmetry energy expression therefore already includes a component of the Wigner term. Any departures indicate contributions beyond the shell model. While the above behavior for nuclei with  $N = Z$  was found to be compatible with the Wigner supermultiplet model, the prevailing spin-orbit interaction in heavier nuclei breaks the spin-isospin symmetry implied by the model, hence  $LS$ -coupling is superceded by  $jj$ -coupling. Lunney et al. [1] suggested that a more direct description of the Wigner effect is likely due to isoscalar  $n$ - $p$  pairing as outlined e.g. by Satula and Wyss [33–36]. Complete mixing between  $T = 1$  and  $T = 0$   $n$ - $p$  pair interactions has been predicted for this region by Goodman [37,38].

The results shown in Figs. 1 to 5 for the predicted values of  $a(A, T)$  suggest that a similar effect with enhancements near  $N \approx Z$  may also be present in the diagonal shell-model regions ( $d_4$ ) and ( $d_5$ ).

Equations (h) and (i) are both derived from the Garvey–Kelson mass relations [27–29] which are based on an independent particle picture and hence on identical underlying principles. Both equations give very good results over the region of experimental data except for a small group of nuclei near  $N \approx Z$  where in region ( $d_3$ ) only equation (i) agrees with the experimentally enhanced coefficients  $a(A, T)$ . This surprising result demonstrates that the mathematical algorithms used in applying the above mass relation seems to have important consequences. The results for equation (h) are based on the technique of ensemble averaging. The results for equation (i) are based on the solutions of a homogeneous partial difference equation. Differences in the predictions for the two approaches are also seen in Figs. 12 and 13. For nuclei with  $A = 164$  beyond  $T = 13$  only equation (i) shows the experimentally observed cusp. On the other hand, for nuclei with  $A = 208$  the predicted slow increase of  $a(A, T)$  beyond  $T = 22$  for equation (i) seems to be at variance with most other mass equations.

As pointed out in the previous section, equation (j) experiences major difficulties particularly for several regions of very proton-rich and neutron-rich nuclei. This is apparent in Fig. 5 and Figs. 7 through 13. Equation (j) is based on the solution of an inhomogeneous partial difference equations [25]. The problems seem to be related to an inadequacy of the isospin dependent cubic source term despite valid arguments in its support. It became clear [39] that an inhomogeneous source term related to the nuclear deformation should have been used instead.

Shell structures in  $a(A, T)$  are observed for all equations except for equation (k). While based on a generalized infinite nuclear matter formula [26], in its application so-called local energy corrections are introduced related to a network of partial difference equations. Equation (k) is therefore a multi-parameter equations. As a consequence all shell structures are quenched in the symmetry energy coefficients  $a(A, T)$ . A detailed discussion of the infinite nuclear mass formula has been presented by Lunney et al. (Ref. [1], p. 1064).

Pairing energies  $P(A, T)$  of Fig. 6 also display variations between the calculated and experimental values and also between each other. However, pairing is an added quantity and therefore of less importance with regard to mass extrapolations. The experimental and essentially all theoretical values show the enhanced pairing quantity for magic nuclei which, as noted above, is a consequence of the discontinuities in symmetry energy at major shell crossings and unrelated to pairing. The decreased pairing observed experimentally for deformed nuclei in the non-diagonal shell region ( $n_5$ ) is reproduced by only one equation, and another equation shows enhanced pairing in heavy nuclei away from magic numbers in disagreement with the experimental data.

### 6.3. Reliability criteria

A common procedure for testing mass equations consist of the comparison between newly measured and predicted mass values. One such comparison is included in the review by Lunney, Pearson and Thibault [1]. Here, the authors determined the root-mean-square errors  $\sigma$  of the fits given by several mass equations to the 1995 atomic mass evaluation [16] and to a 2001 atomic mass evaluation [40]. In addition so-called model standard deviations  $\sigma_{\text{mod}}$  were obtained for 382 new mass values included in the 2001 mass evaluation. The systematic mass values given by Audi and Wapstra [16] give by far the best predictions with  $\sigma_{\text{mod}} = 122$  keV. This is followed among the mass equations considered in Ref. [1] by equation (f; 1995) with 378 keV, equation (i; 1988) with 451 keV, equation (c; 1988) with 485 keV, and equation (d; 1996) with 511 keV. The authors

emphasise the ratios  $R = \sigma_{\text{mod}}/\sigma(1995)$  as shown in their Fig. 13 and Table I even though the basis uncertainties  $\sigma(1995)$  differ by up to a factor of three.

In interpreting such results one must keep in mind that the above new mass values are limited to regions of nuclei which became accessible to measurements in the *interim* and are therefore usually located close to the already known nuclei (see Fig. 4 in Ref. [1]). They do not necessarily provide information for long-range extrapolations far away from the known nuclei particularly into regions of very neutron-rich nuclei such as nuclei involved in the astrophysical r-process in the regions  $100 < A < 125$  and  $A > 150$  [30]. Standard deviations for describing the masses of unknown nuclei increase with the distance from the known nuclei. This increase in standard deviations for actually measured mass values with distance from a given data base has previously been studied for one particular mass equation [41]. In order to establish reliability criteria for long-range extrapolations based on mass equations one needs to investigate the underlying physical principles, as was done in great detail by Lunney, Pearson and Thibault [1], and by considering global characteristics of the mass surfaces generated by the various mass equations including higher-order effects, as is done in the present work.

## 7. Summary

The study of the differences  $\Delta_{T',T}(A)$  between the excitation energies in a given nucleus of isobaric analog states for different values of isospin provides a powerful tool for obtaining a global understanding of the systematics of symmetry and pairing energies in atomic nuclei and hence atomic masses and binding energies.

Symmetry energy coefficients  $a(A, T)$  and pairing energies  $P(A, T)$  have been obtained from experimental mass data and were also derived from eleven selected mass equations. The comparison between these quantities was found to provide information about the quality and possible shortcomings of the theoretical approaches for predicting masses of unknown nuclei. This fact makes the procedure useful for evaluating mass equations particularly since the quantity  $a(A, T)$  is related to the curvature with respect to increasing neutron excess of the nuclear mass surface. While consistency between theoretical and experimental quantities is indicated over wide ranges of nuclei, important deviations also exist for some of the theoretical approaches as outlined and discussed in the preceding sections.

## Acknowledgements

Discussions with K.T. Hecht and N. Zeldes are greatly appreciated. Most sets of calculated mass data were provided by G. Audi. Thanks are due to S.J. Richardson for help with graphics.

## References

- [1] D. Lunney, J.M. Pearson, C. Thibault, Rev. Mod. Phys. 75 (2003) 1021.
- [2] Y. Aboussir, J.M. Pearson, A.K. Dutta, F. Tondeur, Nucl. Phys. A 549 (1992) 155.
- [3] P. Möller, J.R. Nix, W.D. Myers, W.J. Swiatecki, At. Data Nucl. Data Tables 59 (1995) 185.
- [4] J. Duflo, A.P. Zuker, Phys. Rev. C 52 (1995) R23.
- [5] J. Duflo, A.P. Zuker, Phys. Rev. C 59 (1996) R2347.
- [6] J. Jänecke, T.W. O'Donnell, Eur. Phys. J. A 25 (1) (2005) 79.
- [7] J. Jänecke, T.W. O'Donnell, V.I. Goldanskii, Phys. Rev. C 66 (2002) 024327.
- [8] J. Jänecke, T.W. O'Donnell, V.I. Goldanskii, Nucl. Phys. A 728 (2003) 23.
- [9] M.S. Antony, A. Pape, J. Britz, At. Data Nucl. Data Tables 66 (1997) 1.
- [10] G. Audi, A.H. Wapstra, C. Thibault, Nucl. Phys. A 729 (2003) 337.

- [11] J. Jänecke, in: D.H. Wilkinson (Ed.), *Isospin in Nuclear Physics*, North-Holland, Amsterdam, 1969, pp. 298–387, Chapter 8.
- [12] A. deShalit, I. Talmi, *Nuclear Shell Theory*, Academic Press, 1963.
- [13] K.T. Hecht, *Nucl. Phys. A* 102 (1967) 11.
- [14] I. Talmi, *Simple Models of Complex Nuclei*, Harwood Academic Publishers, 1993.
- [15] S. Liran, N. Zeldes, *At. Data Nucl. Data Tables* 17 (1976) 431.
- [16] G. Audi, A.H. Wapstra, *Nucl. Phys. A* 595 (1995) 409.
- [17] J. Jänecke, T.W. O'Donnell, *Phys. Lett. B* 605 (2005) 87.
- [18] A.H. Wapstra, G. Audi, C. Thibault, *Nucl. Phys. A* 729 (2003) 129.
- [19] E.P. Wigner, *Phys. Rev.* 51 (1937) 106.
- [20] P. Möller, J.R. Nix, *At. Data Nucl. Data Tables* 39 (1988) 213.
- [21] W.D. Myers, W.J. Swiatecki, *Nucl. Phys. A* 601 (1996) 141.
- [22] T. Tachibana, M. Uno, M. Yamada, S. Yamada, *At. Data Nucl. Data Tables* 39 (1988) 251.
- [23] E. Comay, I. Kelson, A. Zidon, *At. Data Nucl. Data Tables* 39 (1988) 235.
- [24] J. Jänecke, P.J. Masson, *At. Data Nucl. Data Tables* 39 (1988) 265.
- [25] P.J. Masson, J. Jänecke, *At. Data Nucl. Data Tables* 39 (1988) 273.
- [26] L. Satpathy, R.C. Nayak, *At. Data Nucl. Data Tables* 39 (1988) 241.
- [27] G.T. Garvey, I. Kelson, *Phys. Rev. Lett.* 16 (1966) 197.
- [28] G.T. Garvey, W.J. Gerace, R.L. Jaffee, I. Talmi, I. Kelson, *Rev. Mod. Phys.* 41 (1969) S1.
- [29] G.T. Garvey, *Annu. Rev. Nucl. Sci.* 19 (1969) 433.
- [30] Rare Isotope Accelerator (RIA), <http://www.orau.gov/ria>.
- [31] W.D. Myers, W.J. Swiatecki, *Nucl. Phys.* 81 (1966) 1.
- [32] W.D. Myers, *Droplet Model of Atomic Nuclei*, IFI/Plenum, New York, 1977.
- [33] W. Satula, R. Wyss, *Phys. Lett. B* 393 (1997) 1.
- [34] W. Satula, D.J. Dean, J. Gary, S. Mizutori, W. Nazarewicz, *Phys. Lett. B* 407 (1997) 103.
- [35] W. Satula, R. Wyss, *Nucl. Phys. A* 676 (2000) 120.
- [36] W. Satula, R. Wyss, *Phys. Rev. Lett.* 87 (2001) 52504.
- [37] A.L. Goodman, *Phys. Rev. C* 58 (1998) R3051.
- [38] A.L. Goodman, *Phys. Rev. C* 60 (1999) 014311.
- [39] J. Jänecke, K. Ashktorab, unpublished contribution to AMCO9 (1990).
- [40] G. Audi, A.H. Wapstra, private communications to Lunney et al. [1].
- [41] J. Jänecke, E. Comay, *Nucl. Phys. A* 436 (1985) 108.